PAPER Special Section on Recent Progress in Antennas, Propagation and Wireless Systems Related to Topics in ISAP2014

Four-Stream Parallel Transmission for Short-Range MIMO Using Only Passive Analog Components

Kentaro MURATA[†a)], ***Student Member***, **Naoki HONMA**[††], ***Member***, **Kentaro NISHIMORI**[†††], ***Senior Member***, **David M. KLYMYSHYN**[††††], ***Nonmember***, ***and*** **Hisashi MORISHITA**[†], ***Fellow***

SUMMARY An analog-beamforming-based eigenmode transmission technique is proposed that employs a network of interconnected 180-degree hybrid couplers at both transmitting and receiving sides of a plane-symmetrically configured short-range MIMO system. This technique can orthogonalize MIMO channels regardless of array parameters such as antenna spacing and Tx-Rx distance, provided the MIMO array is symmetric. For verifying the effectiveness of the proposed technique in channel orthogonalization, an experiment is conducted using a 4×4 MIMO array consisting of microstrip antennas and cascade-connected rat-race hybrid couplers. The results indicate a reduction in interference by approximately −28.3 dB on average compared to desired signal power, and the ability to realize four-stream parallel MIMO transmission by using only analog passive networks. The proposed technique can achieve channel capacity almost equivalent to that of eigenbeam space division multiplexing with ideal digital beamforming.

key words: *short-range MIMO, eigenmode transmission, 180-degree hybrid coupler*

1. Introduction

Recently, contactless card services have become very popular in transportation and electronic payment systems. Moreover, radio frequency identification (RFID) technology is finding increased application in manufacturing and logistics [1]. As typified by these applications, short-range communication technology is playing an indispensable role in today's ubiquitous society. With the rapid development of infrastructures for machine-to-machine communication, cloud-computing-based content distribution services such as data downloading from digital KIOSKs have been commercialized, and higher-speed short-range wireless communication capable of large-capacity data transfer such as music, movies and images will be highly demanded in the near future. However, since conventional short-range communication schemes used for RFID are limited to lower-capacity applications, communication speed is a critical bottleneck hindering large-capacity communications. Currently, the utilization of ultra wide band and millimeter wave technologies are a focus for large-capacity short-range wireless communications with maximum data rates reaching up to multiple Gbits/s [2].

Another alternative is to employ multiple-input multiple-output (MIMO) technology. Short-range MIMO (SR-MIMO) is an emerging utility form of MIMO technology, expected to be applied, for example, to a through-the-wall repeater [3], [4]. Conventionally, MIMO systems are operated in rich spattering environments and improve wireless communication speed and quality by the use of diversity effects and spatial multiplexing [5]. In contrast, Paulaj pointed out that, even when the line-of-sight (LOS) component is dominant in a MIMO channel, a channel capacity higher than the ergodic capacity of a traditional MIMO scheme operated in a rich-scattering environment can be achieved under the specific condition that the LOS channel components are initially uncorrelated. This hints at the possible effectiveness of LOS MIMO communication from the linear algebraic viewpoint [6].

Considering this point, optimal array designs for LOS MIMO that provide uncorrelated channels were investigated based on plane and spherical wave theories. For instance in [7]–[10], MIMO array antenna spacing is regarded as a key factor to realize uncorrelated channels when Tx-Rx distance is fixed. It was proven that a full-rank channel matrix can be realized by arranging MIMO array antenna elements at optimal spacing intervals. This research confirms the hypothesis presented in [6] and validates the effectiveness of LOS MIMO, in the other words, SR-MIMO from an electromagnetic perspective.

As the concept of SR-MIMO became popular, research tackled challenges to enhance communication performance. In [11] and [12], propagation characteristic improvement techniques using scatterers such as reflectors and metal wires were proposed. Although these approaches are somewhat straightforward, signal to noise ratio (SNR) can be substantially improved by controlling back and side lobes and beam width, simply by optimizing the sizes and positions of scatterers around an SR-MIMO array. From these earlier studies including [6]–[12], a suitable design method of array configuration for SR-MIMO systems has matured.

A current focus in practical use of SR-MIMO technology involves channel multiplexing with simpler hardware-software configurations. Broadly, conventional channel multiplexing techniques for SR-MIMO are classified into

Manuscript received April 6, 2015.
Manuscript revised August 17, 2015.

[†]The authors are with Graduate School of Science and Engineering, National Defense Academy, Yokosuka-shi, 239-8686 Japan.
[††]The author is with Faculty of Engineering, Iwate University, Morioka-shi, 020-8551 Japan.
[†††]The author is with Faculty of Engineering, Niigata University, Niigata-shi, 950-2181 Japan.
[††††]The author is with Department of Electrical Engineering, University of Saskatchewan, Canada.
a) E-mail: ed14002@nda.ac.jp

DOI: 10.1587/transcom.2015ISP0028

three categories.

The first category proposes a multiplexing technique utilizing orthogonal polarizations. In MIMO communications, it is widely accepted that polarization waves allow spatially uncorrelated MIMO channels in a far region. For example, when triple polarizations are employed, an ideal three-fold channel capacity is expected compared with a single polarization [13]. In [14] and [15], dual-polarization multiplexing techniques for SR-MIMO were reported. These studies clarified that lower order eigenvalues of the channel matrix were significantly improved by applying dual-polarization that contributed to the channel capacity improvement. The use of a dual-polarized microstrip antenna (MSA) also helped to miniaturize a MIMO array system. As these findings suggested, it was verified that polarization multiplexing was also effective in SR-MIMO communication.

In the second category, a channel multiplexing method that used electric and magnetic modes in a near-field region as distinct information carriers was proposed [16], [17]. This method exploits the characteristic of a reactive near field where attenuation rates of electric and magnetic fields radiated from small electric and magnetic dipoles are different. This multiplexing mechanism is completely different from polarization.

The greatest benefit of the first two categories is that, since only polarized or electric/magnetic antennas are used, multiplexed channels can be easily constructed by an extremely simple system configuration without specialized RF front-ends for signal separation. However, the maximum level of multiplexing possible is electromagnetically limited to three (by tri-polarization) and two (by electric and magnetic fields). Therefore, a different approach must be taken for multiplexing channels of the same polarizations or fields.

The third category involves analog-beamforming-based decoding techniques. Usually, short-range communication links are static since Tx and Rx antennas exist in the LOS environment. Therefore, propagation channels are uniquely determined, that enables a fixed-weight decoding. In the previous studies, analog decoding techniques using passive circuit elements (such as dividers, phase shifters and attenuators) [18], [19], sub-arrays [20] and orthogonal-directivity antennas [21] were proposed. The merits of the use of analog-beam forming are: 1) high frequency utilization efficiency; and 2) low power consumption due to broadband characteristics and passive analog circuits. However, a problem with analog-beamforming is that the array displacement causes a capacity degradation since a fixed-weight analog beamformer cannot form an optimal beam adaptively in response to the array displacement unlike with conventional digital beamforming.

To solve this problem, the authors proposed a novel eigenmode transmission technique using only 180-degree hybrid couplers [22]. In this technique, as long as the symmetry of the MIMO array configuration is retained, it is possible to orthogonalize MIMO channels regardless of array parameters such as the type of antenna, antenna spacing and Tx-Rx distance. Therefore, this technique is robust to specific direction displacements and specific rotation angles of the MIMO array.

In related work, the authors also proposed a simultaneous matching technique for SR-MIMO considering the influence of the proximally-positioned Tx and Rx arrays [23], and this novel matching theory is founded upon the concept of the proposed channel orthogonalization technique. After the channel orthogonalization, the SR-MIMO system can be regarded as multi independent single-input single-output (SISO) systems. Then corresponding pairs of Tx and Rx ports can be simultaneously matched by applying conjugate-image-impedance theory to each orthogonalized SISO system individually, that extracts the maximum channel capacity that an arbitrary SR-MIMO potentially possesses. Furthermore, it was reported that although the application limitation of the channel orthogonalization technique was up to 4×4 MIMO when Tx and Rx arrays faced each other (usual for short-range communication), this approach could be extended to a massive SR-MIMO system consisting of many more antennas. Combining this technique with digital beamforming results in a considerable reduction of calculations required for eigenbeam space division multiplexing (E-SDM) [24].

In our previous work, it was demonstrated experimentally that this base channel orthogonalization technique achieved a channel capacity almost equivalent to that of digital-beamforming-based E-SDM in a 2×2 SR-MIMO system [25], [26]. However, although the extension method to more than a 2×2 SR-MIMO was theoretically established, the effectiveness of it was not experimentally demonstrated.

The purpose of the paper is to validate the effectiveness of the proposed technique in a 4×4 SR-MIMO system operating in an actual environment. In the experiment, MSA arrays and cascade-connected networks consisting of four rat-race couplers were used for setting up the proposed SR-MIMO system. In this paper, some experimental results are presented, and the channel orthogonalization effect and channel capacity improvement are quantitatively evaluated. These results confirm that the four-stream parallel MIMO transmission can be successfully achieved using fairly simple analog passive networks. Finally, this paper proves that the proposed technique of analog-based E-SDM (AE-SDM) can achieve a channel capacity almost equivalent to that of digital-based E-SDM (DE-SDM) by ideal beamforming in a 4×4 SR-MIMO system.

2. Theory of Proposed Technique

In this section, the extension method of AE-SDM to a 4×4 SR-MIMO system is explained. Details on the fundamental theory of the proposed technique can be found in [22].

A 4×4 SR-MIMO system with a cuboidal configuration, symmetrical with respect to the vertical and horizontal reference planes is shown in Fig. 1. In the system, transmitting antennas Tx 1∼4 are connected to Tx ports #1∼#4, and receiving antennas Rx 1∼4 are connected to Rx ports

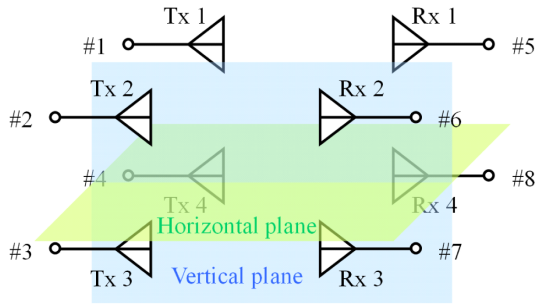

Fig. 1 Plane-symmetrically configured 4×4 SR-MIMO system.

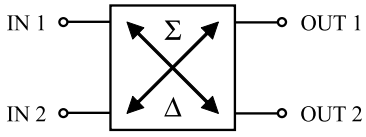

Fig. 2 Symbol of an 180-degree hybrid coupler.

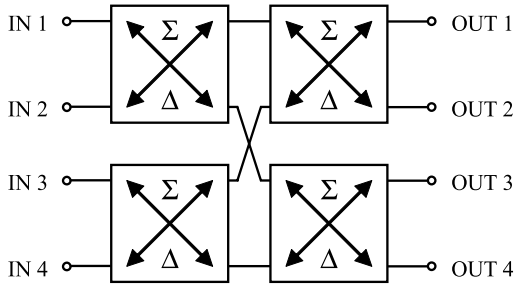

Fig. 3 Network configuration of a cascaded-connected couplers.

#5~#8. The channel matrix of the system, $\boldsymbol{S}_{\mathrm{chl}}$, is expressed with port numbers as

$$\boldsymbol{S}_{\mathrm{chl}} = \begin{bmatrix} S_{51} & S_{52} & S_{53} & S_{54} \\ S_{61} & S_{62} & S_{63} & S_{64} \\ S_{71} & S_{72} & S_{73} & S_{74} \\ S_{81} & S_{82} & S_{83} & S_{84} \end{bmatrix} \tag{1}$$

where, for example, S_{51} is a channel between Tx port #1 and Rx port #5.

Due to the symmetry of the array configuration, channels between 1) ports facing each other, 2) ports existing across the vertical plane, 3) ports existing across the two planes and 4) ports across the horizontal plane are equal and replaced with α, β, γ and δ, respectively. This makes

$$\boldsymbol{S}_{\mathrm{chl}} = \begin{bmatrix} \alpha & \beta & \gamma & \delta \\ \beta & \alpha & \delta & \gamma \\ \gamma & \delta & \alpha & \beta \\ \delta & \gamma & \beta & \alpha \end{bmatrix} \tag{2}$$

a regular symmetrical matrix.

Cascade-connected couplers (CCC) used in the propose technique are constructed by cascade-connecting four hybrid couplers as shown in Fig. 3. Note that input ports IN 1 and IN 2 of a single hybrid coupler shown in Fig. 2 correspond to even and odd modes. A signal input to IN 1 is equally split to output ports OUT 1 and OUT 2 in phase, while a signal input to IN 2 is output in reversed phase [27]. Taking this matter into consideration, the transmission matrix between inputs and outputs of an ideal CCC, $\boldsymbol{S}_{\mathrm{CCC}}$, is expressed as

$$\boldsymbol{S}_{\mathrm{CCC}} = -\frac{1}{2}\begin{bmatrix} 1 & 1 & 1 & 1 \\ 1 & 1 & -1 & -1 \\ 1 & -1 & 1 & -1 \\ 1 & -1 & -1 & 1 \end{bmatrix}. \tag{3}$$

An ideal hybrid coupler has neither reflection nor mutual coupling in both inputs and outputs, and this is also true for CCC.

Two CCCs are connected to both Tx and Rx sides of the plane-symmetrically configured 4×4 SR-MIMO system. Inputs IN 1~4 and outputs OUT 1~4 of Tx CCC are connected to Tx ports #1~#4 and transmitting antennas Tx 1~4, respectively. Inputs IN 1~4 and outputs OUT 1~4 of Rx CCC are connected to receiving antenna Rx 1~4 and Rx ports #5~#8, respectively. Since the networks have no reflection or mutual coupling, the complete cascade-connected transmission matrix can be expressed as the product of the transmission matrices of the individual networks [28]. Thus, the ideal channel matrix of the whole SR-MIMO system including the cascade-connected Tx and Rx CCCs, $\boldsymbol{S}'_{\mathrm{chl}}$, is given as

$$\boldsymbol{S}'_{\mathrm{chl}} = \boldsymbol{S}_{\mathrm{CCC}}\boldsymbol{S}_{\mathrm{chl}}\boldsymbol{S}_{\mathrm{CCC}}. \tag{4}$$

By substituting (2) and (3) into (4), we obtain

$$\boldsymbol{S}'_{\mathrm{chl}} = \begin{bmatrix} S'_{51} & S'_{52} & S'_{53} & S'_{54} \\ S'_{61} & S'_{62} & S'_{63} & S'_{64} \\ S'_{71} & S'_{72} & S'_{73} & S'_{74} \\ S'_{81} & S'_{82} & S'_{83} & S'_{84} \end{bmatrix}$$

$$= \begin{bmatrix} \alpha+\beta+\gamma+\delta & 0 & 0 & 0 \\ 0 & \alpha+\beta-\gamma-\delta & 0 & 0 \\ 0 & 0 & \alpha-\beta+\gamma-\delta & 0 \\ 0 & 0 & 0 & \alpha-\beta-\gamma+\delta \end{bmatrix} \tag{5}$$

and the channel matrix is diagonalized. That means that four orthogonalized streams are formed between corresponding pairs of Tx and Rx ports, and E-SDM is realized.

As discussed above, orthogonalized channels can be formed between corresponding Tx and Rx ports using CCCs, and the proposed technique allows E-SDM using only analog passive networks without digital beamforming. For reference, this technique is valid regardless of antenna spacing and Tx-Rx distance as long as the symmetry of the array configuration is retained.

3. Experimental Results

In this section, evaluation results on the effect of channel orthogonalization and the channel capacity improvement by the proposed technique are shown.

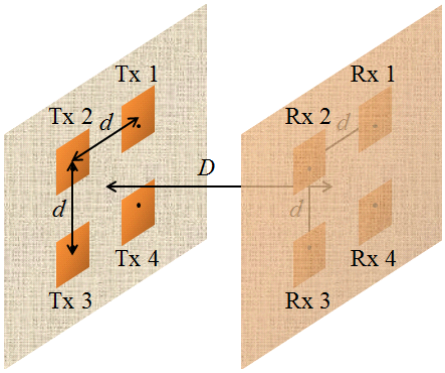

Fig. 4 Configuration of a 4×4 MSA SR-MIMO array.

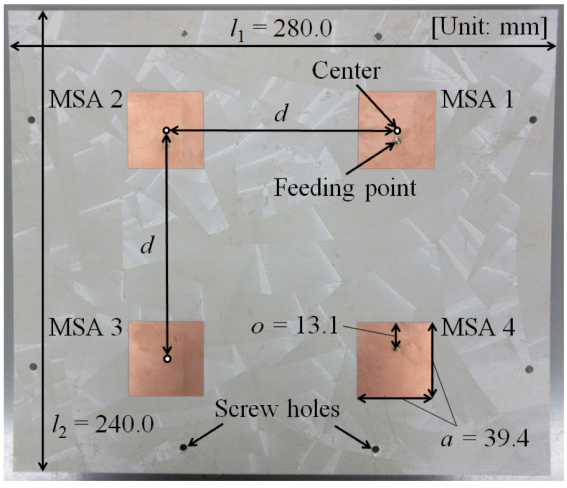

Fig. 5 Four-element MSA array.

3.1 Experimental Setup

3.1.1 Array Configuration

In Fig. 4, the configuration of the experimental 4×4 SR-MIMO array is illustrated. Both Tx and Rx arrays consist of four identical MSAs. Figure 5 is a picture of a fabricated MSA array on a polytetrafluoroethylene (PTFE) substrate with thickness of 1.56 mm and relative permittivity of 2.2. The size of the substrate is as shown in the figure. Such a large ground plane has two potential effects 1) to reduce scattering waves by screening the objects behind the array such as CCC and cables, and 2) to assure a highly accurate symmetry by employing the co-planar array configuration. However in principle, the size of the ground plane does not affect the proposed channel orthogonalization on the condition that the plane symmetry of the SR-MIMO array configuration is kept. Actually, a sufficient channel orthogonality was experimentally confirmed even by using arrays consisting of separated MSAs with small ground plane [25], [26]. The size of each MSA and its feeding point are optimized so that a single MSA assumed on the infinite dielectric substrate is fully matched at the center frequency of

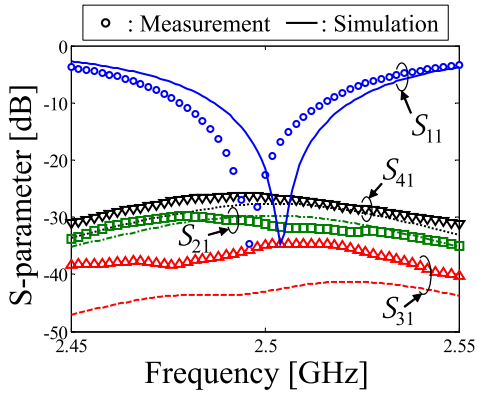

Fig. 6 Frequency responses of S-parameter.

2.5 GHz. The array has eight screw holes for fixture mounting (see Fig. 10). In terms of array parameters, antenna spacing, d, is defined as the distance between the centers of the MSAs, and Tx-Rx distance, D, is defined as the distance between the grounds of Tx and Rx arrays. In order to evaluate antenna spacing characteristics, three types of the arrays whose d is 0.8, 1.0 and 1.2 λ were fabricated, where λ is the free-space wavelength at the center frequency.

For reference, the S-parameter frequency responses of the array with $d = 1.0\lambda$ are shown in Fig. 6. In the figure, characteristics for only MSA 1 are shown because of the structural symmetry, and S_{11}, S_{21}, S_{31} and S_{41} represent the reflection of MSA1, and the couplings with MSA 2~4, respectively. Bold and thin lines are measurement and simulation results, respectively, and in the simulation, an infinite dielectric plane was assumed as a dielectric layer of the array substrate for the convenience of calculation. For electromagnetic analysis, IE3D was used [34]. From the figure, although it is observed that the measurement resonant point is shifted to lower frequency compared with that of simulation because of the difference in dielectric layer, the reflection is −22.7 dB, suppressed to a satisfactory extent at the center frequency. Also, couplings with the other element are reduced to under −26.5 dB at the center frequency. Likewise, for the arrays with $d = 0.8$ and 1.2 λ, it is confirmed that reflections and couplings are held under the sufficiently low levels of −13.5 and −23.4 dB, respectively, therefore, these characteristics are omitted from the paper.

Additionally, Figs. 7(a) and (b) show E- and H-plane (zx- and xy-plane) radiation patterns of MSA1 of the array with $d = 1.0\lambda$; those of MSA2~4 should be symmetrical to that of MSA1 so they are omitted. The array exists right on the yz-plane and its center is located at the origin of the coordinate. θ and ϕ are defined as the right-handed angle from z-axis and the left-handed angle from x-axis, respectively. In the figures, measured E_θ and E_ϕ components are normalized by maximum E_θ on each plane, and plotted with circle and square markers, respectively. Also, simulated E_θ is normalized by its maximum and shown in bold line while simulated E_ϕ is omitted since it is negligibly small. From the experimental results, the peak gains of E- and H-plane patterns

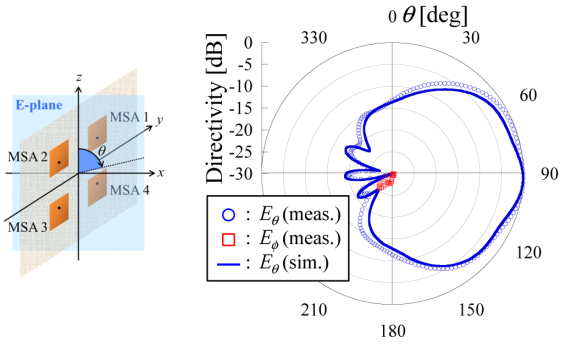

(a) E-plane (*zx*-plane).

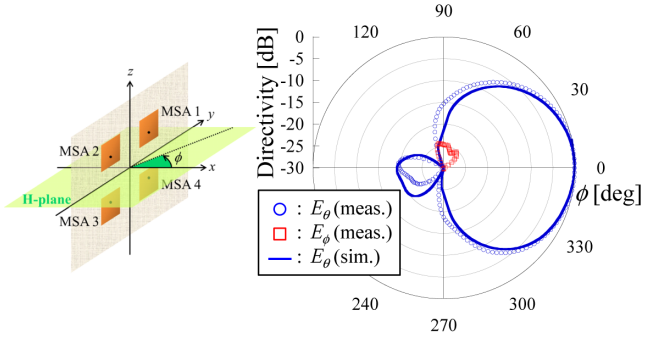

(b) H-plane (*xy*-plane).

Fig. 7 Radiation pattern.

are 7.87 dBi at $\theta = 95.4$ degree and 8.18 dBi at $\phi = 358.4$ degree, respectively. And, their half-value angles are 91.2 and 79.2 degrees, respectively. The figures show that the experimental patterns are in good agreement with those of the simulation. Note, however, that these far-field characteristics are not necessarily directly-reflected in the following analysis results for such short-range cases.

3.1.2 Cascade-Connected Couplers

Rat-race hybrid couplers with details shown in Figs. 8 and 9 are used for implementation. λ_{eff} (87.8 mm) is the effective wavelength at the center frequency calculated considering the thickness and the relative permittivity of the dielectric substrate [29]. The width of the line of the rat-race, w_{r}, was determined for a characteristic impedance of $\sqrt{2}Z_0$ based on [29], where Z_0 is 50 Ω. The fabricated hybrid coupler has connectors on its back side, and is connectable to MSA arrays and measuring instruments via flexible cables. A fabricated CCC configured with four concatenated rat-races is shown in Fig. 9. In Table 1, the input-output characteristics of the fabricated CCC at the analysis frequency are shown. Table 1(a) shows amplitude characteristics in dB. Although a slight loss occurs in each component, the input signal is equally split to four outputs. Table 1(b) shows phase characteristics. The absolute value of the relative phase of each output signal to OUT 1 is displayed in degrees. From the table, it is found that phase characteristics with low error are

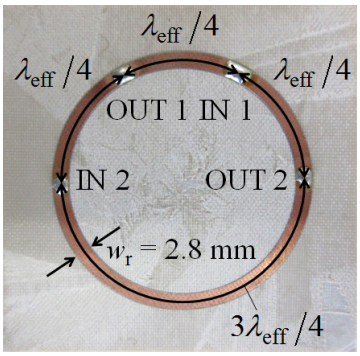

Fig. 8 Fabricated rat-race.

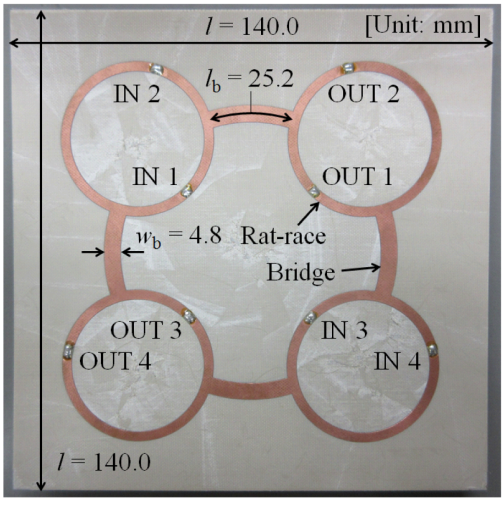

Fig. 9 Fabricated CCC.

Table 1 Input-output characteristics.

(a) Amplitude

Unit: dB	IN 1	IN 2	IN 3	IN 4
OUT 1	−6.25	−6.24	−6.27	−6.24
OUT 2	−6.21	−6.22	−6.23	−6.24
OUT 3	−6.27	−6.22	−6.33	−6.26
OUT 4	−6.26	−6.24	−6.25	−6.23

(b) Relative phase

Unit: deg	IN 1	IN 2	IN 3	IN 4
OUT 1	0	0	0	0
OUT 2	0.27	0.10	179.76	179.88
OUT 3	0.82	179.20	0.53	179.52
OUT 4	1.09	179.02	179.13	0.74

obtained, compared to the ideal CCC shown in (3).

Although such a bulky circuit structure was used in the experiment for fundamental performance validation of the proposed technique, further miniaturization of CCC is necessary from a practical application standpoint. In [30] and [31], distributed circuits similar to CCC used in the proposed technique are presented, using 3-dB quadrature hybrids and delay lines as a substitute for 180-degree hybrid

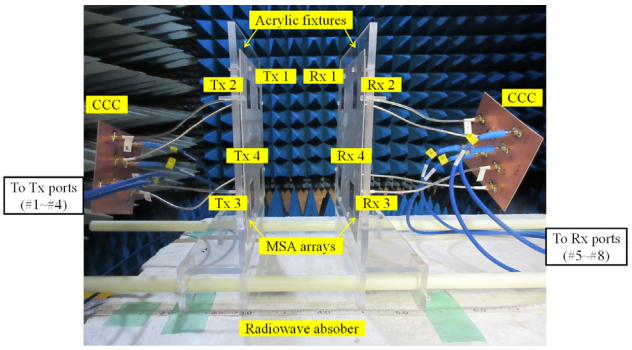

Fig. 10 Picture of an experimental setup.

couplers. In [32], a lumped-element quadrature coupler fabricated using deep X-ray lithography process is presented, enabling approximately 85% area reduction compared to a conventional quadrature hybrid. Thus, drastic miniaturization of the proposed system configuration can be expected through the use of novel circuit structures and fabrication techniques.

3.1.3 SR-MIMO System Configuration

Figure 10 shows the 4×4 SR-MIMO system configuration used in the experiment. The experiment was conducted in a reverberation room. Tx and Rx arrays were fixed on acrylic fixtures and faced each other. The Tx and Rx fixtures were designed so either could be slid along the Tx-Rx distance direction to obtain the MIMO channel characteristics versus distance. In the experiment, two patterns of MIMO channels were measured; first, the channel matrix was obtained when a measuring instrument was directly connected to the SR-MIMO array without CCCs. Second, the channel matrix was obtained with CCCs connected as shown in Fig. 10. The observed frequency range is ±50 MHz from the center frequency, and the noise level is approximately −90 dBm, which is almost equal to that at room temperature (300 K) calculated by the Johnson-Nyquist formula [33].

3.2 The Effect of a Channel Orthogonalization

In order to exhibit the effect of the channel orthogonalization, the amplitudes of MIMO channel components measured by a vector network analyzer (VNA) are visualized in gray scale in Fig. 11. In the experiment, the Tx and Rx arrays whose d is 1.0 λ were used and D was set to 1.0 λ. In the figure, the amplitude is shown in dB, and the upper and lower limits are set to 0 and −30 dB, respectively.

Figure 11(a) is an amplitude characteristic without CCCs, and this figure indicates a regular symmetry expressed as (2) due to the plane-symmetry of the SR-MIMO system configuration. In the figure, diagonal components represent desired signal channels between corresponding Tx and Rx ports, while non-diagonal components in each row represent interference channels from non-corresponding Tx ports to a certain Rx port. Hence, in the case that CCCs are

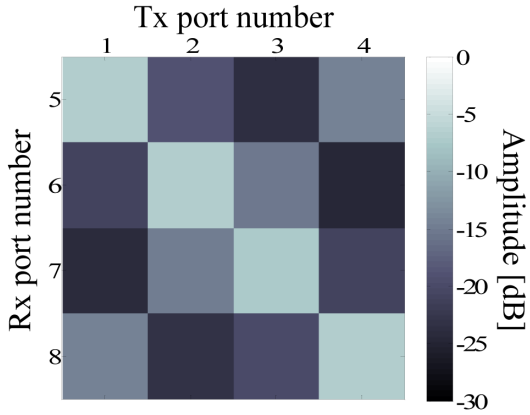

(a) w/o CCCs

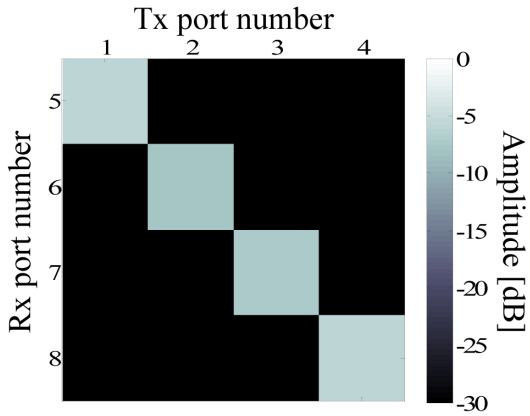

(b) w/ CCCs

Fig. 11 Visualization of channel components.

not connected, interferences noticeably exist at the similar level to signal channels, and because of this, signal to interference and noise power ratio (SINR) in each stream is poor.

On the other hand, Fig. 11(b) shows a channel characteristic with CCCs. From the figure, it is confirmed that only diagonal components, or signal channels, remain while non-diagonal components, or interference channels, are reduced below −30 dB. On the basis of these results, it is confirmed that the proposed technique can reduce interference from non-corresponding Tx to a sufficient extent.

3.3 Signal and Interference Characteristics

In this subsection, signal and interference powers in each stream are evaluated more quantitatively. In the measurement, the same arrays as described in 3.2 were used, and D was varied from 0.5 to 2.0 λ at 0.25-λ intervals. For comparison, simulation results are also shown. In the simulation, the array parameters were set to same values as those in the experiment, and D was varied over the same range but more finely at 0.05-λ intervals.

In Fig. 12, three types of signal powers are displayed;

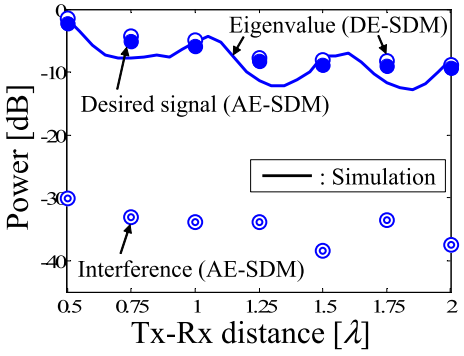

(a) First stream

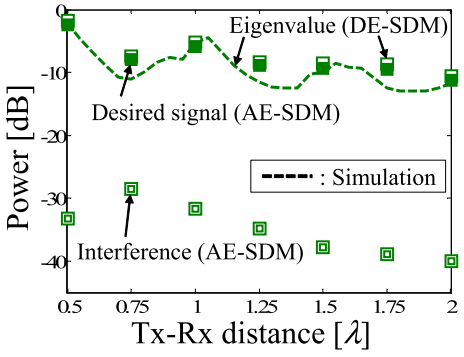

(b) Second stream

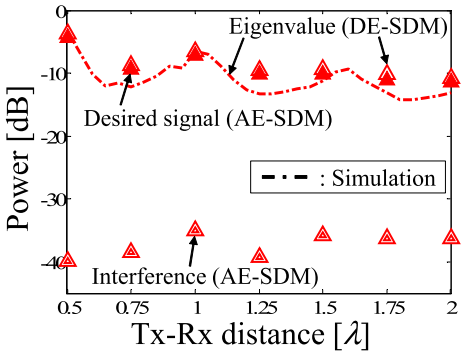

(c) Third stream

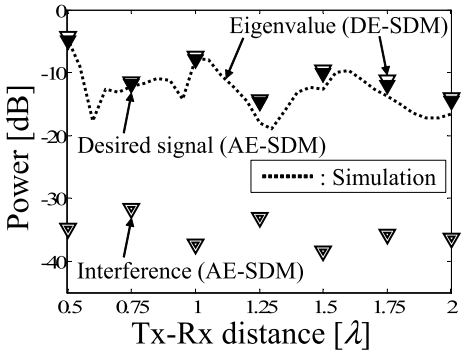

(d) Fourth stream

Fig. 12 Experimental results on signal and interference powers.

the first is a signal power when DE-SDM is applied to a numerically-simulated channel matrix, and defined eigenvalue of a correlation matrix of the channel matrix. The second is a signal power when DE-SDM is applied to an experimentally-measured channel matrix without CCCs, and defined in a same manner as the first. The third is a signal power when the proposed AE-SDM is applied, and defined as the square of the absolute value of a diagonal component in an experimentally-measured channel matrix with CCCs. These three types of signals are shown with lines, open and filled markers, respectively. Additionally, the interference when AE-SDM is applied is also shown with double-lined markers, and defined as the square sum of the absolute value of non-diagonal components in a certain row of the channel matrix. Figures 12(a)~(d) present the characteristics of the first to fourth streams, where the order is determined by the signal level of each stream.

First, in comparison between experimental and simulated signal powers, it is confirmed that experimental values are somewhat higher than simulated ones as a whole. As possible causes of that, the following points are cited; 1) an infinite dielectric plane is assumed in the numerical simulation so that the dielectric loss in the dielectric layer increased, and 2) more multi-paths are expected in the experiment due to the scatterers around the arrays such as fixtures and radiowave absorbers so that signal power is enhanced. However, both experimental and simulation results show the similar increase and decrease tendencies in each stream.

When comparing AE-SDM and DE-SDM, almost the same characteristics are obtained. The average signal power deteriorations from the first to fourth streams are extremely slight over the analysis range and retained −0.69, −0.60, −0.70 and −0.49 dB, respectively. The cause of the deterioration is discussed in detail in Appendix in the end of the paper.

Focusing on the interference characteristics, it is confirmed that interference power is suppressed under approximately −30 dB over the analysis range for each stream. As a result, the average signal to interference power ratio (SINR) is 28.3 dB overall, therefore, favorable channel orthogonalization effect is demonstrated.

3.4 Channel Capacity Characteristics

In this subsection, channel capacity characteristics are evaluated. In the experiment, D was varied over the same range as 3.3, and the arrays whose d is $d = 0.8$ and $1.2\,\lambda$ were also used aside from $d = 1.0\,\lambda$. As an evaluation formula, channel capacity is expressed as

$$C = \sum_{i=1}^{N_{\mathrm{Rx}}} \log_2(1 + SINR(i)) \tag{6}$$

where $SINR(i)$ for ith stream is given as

$$SINR(i) = \frac{\left|h_{i,i}\right|^2 P_{\mathrm{t}}/N_{\mathrm{Tx}}}{\sum_{j\neq i,j=1}^{N_{\mathrm{Tx}}} \left|h_{i,j}\right|^2 P_{\mathrm{t}}/N_{\mathrm{Tx}} + P_{\mathrm{n}}}. \tag{7}$$

In the above equation, $h_{i,i}$ is the ith diagonal component of a channel matrix and corresponds to a desired signal channel. On the other hand, $h_{i,j}$ is a non-diagonal component of a channel matrix in the ith row and jth column and corresponds to an interference channel. As for DE-SDM, eigenvalues of a correlation matrix of a channel matrix are substituted into a signal-power term, while an interference-power term is zero. N_{Tx} and N_{Rx} represent the numbers of Tx and Rx antennas, respectively, and equal 4 in the experiment. P_{t} and P_{n} represent total transmission power and receiving noise level, and the ratio of P_{t} to P_{n} is 30 dB.

In Fig. 13, channel capacity characteristics are shown. In the figure, experimental results of DE-SDM, AE-SDM, and w/o BF are shown with different types of markers where w/o BF is a characteristic when no beamforming is done. For reference, simulation results are also shown with different types of lines, and as for AE-SDM of simulation, its capacity is calculated from a numerically-simulated channel matrix multiplied by the transmission matrix of an ideal CCC given in (3).

First, in terms of the simulation results of DE-SDM and AE-SDM, the capacity of AE-SDM should theoretically agree with that of DE-SDM. However, it is confirmed that the AE-SDM characteristics unnaturally deteriorate over the range from 0.75 to 1.0 λ. This is caused since the symmetry of the array configuration cannot be perfectly realized due to the specification of the electromagnetic simulator. As for the reason why the experimental results are slightly higher than those of simulation, it is already discussed in the previous subsection.

Comparisons between AE-SDM and w/o BF over the analysis range of D when d = 0.8, 1.0 and 1.2 λ are 4.30, 3.78 and 2.75 times on average, respectively, shows that channel capacity is drastically improved by the proposed technique. This also indicates that when antenna spacing is smaller, more capacity improvement is expected since larger antenna spacing allows channel separation without beamforming, i.e. when antenna spacing is infinite, completely-independent streams can be formed between corresponding pair of Tx and Rx antennas.

Finally, experimental results of AE-SDM and DE-SDM are compared. As well as signal characteristics shown in the previous section, the characteristic deterioration is observed. However, the average capacity deterioration over the analysis range of D when d = 1.0 λ is only 6.0%, therefore, it is confirmed that E-SDM can be sufficiently realized by the proposed technique independently of Tx-Rx distance. Furthermore, although channel orthogonalization performance is inferior compared to when d = 1.0 λ, capacity deteriorations when d = 0.8 and 1.2 λ are sufficiently small, at 12.0% and 11.7%, respectively. From these results, it is verified that the proposed technique is valid regardless of not only Tx-Rx distance but also antenna spacing.

Despite the array parameter independence of the proposed channel orthogonalization, channel capacity is highly dependent upon SR-MIMO array configuration. For example, a smaller antenna spacing compared to Tx-Rx distance

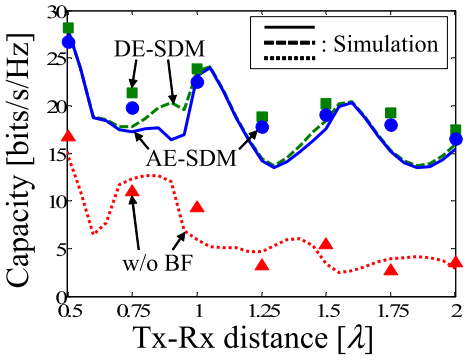

(a) d = 1.0 λ

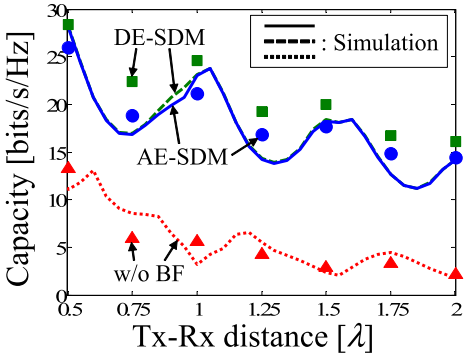

(b) d = 0.8 λ

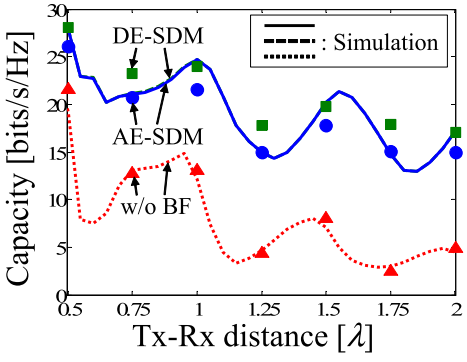

(c) d = 1.2 λ

Fig. 13 Experimental results on channel capacity.

leads to highly correlated channels, which are not suitable for space multiplexing. In addition, a strong mutual coupling between the elements causes SNR deterioration. On the other hand, an infinitely large spacing yields two independent streams but does not always provide the best MIMO performance in an SR-MIMO system in terms of SNR. SR-MIMO has an optimal antenna spacing realizing maximum channel capacity, and optimal Tx-Rx array configurations were theoretically discussed in previous studies [7]–[10]. For practical purposes, the antenna spacing of an SR-MIMO array should be chosen considering a balance between desired communication properties and design size limitation.

4. Conclusion

For the purpose of verifying the effectiveness of the proposed technique in a 4×4 SR-MIMO system, an experiment was conducted using fabricated four-element MSA arrays and CCCs. This paper details the channel orthogonalization effectiveness of the proposed technique as determined from evaluation results.

The results showed that an average interference power can be reduced to −28.3 dB at the average desired power over the analysis range. From the channel capacity characteristics versus Tx-Rx distance when antenna spacing is 1.0 λ, it has been confirmed that the average capacity deterioration by the proposed AE-SDM is only 6.0% compared to DE-SDM, an ideal transmission method for MIMO. Also, the capacity deteriorations for the other antenna spacings are approximately 10%, therefore, the proposed technique allows E-SDM with satisfactory performance independently of antenna spacing and Tx-Rx distance. This has experimentally proven that the proposed technique is also effective in a 4×4 SR-MIMO system.

References

[1] R. Want, "An introduction to RFID technology," IEEE Pervasive Comput., vol.5, no.1, pp.25–33, Jan. 2006.
[2] C. Park and T.S. Rappaport, "Short-range wireless communications for next-generation networks: UWB, 60 GHz millimeter-wave WPAN, And ZigBee," IEEE Wireless Commun., vol.14, no.4, pp.70–78, Aug. 2007.
[3] N. Honma, K. Nishimori, T. Seki, and M. Mizoguchi, "Short range MIMO communication," Proc. 3rd EuCAP, pp.1763–1767, March 2009.
[4] K. Nishimori, N. Honma, T. Seki, and K. Hiraga, "On the transmission method for short-range MIMO communication," IEEE Trans. Veh. Technol., vol.60, no.3, pp.1247–1251, March 2011.
[5] G.J. Foschini and M.J. Gans, "On limits of wireless communications in a fading environment when using multiple antennas," Wireless. Pers. Commun., vol.6, no.3, pp.311–335, 1998.
[6] A. Paulaj, R. Nabar, and D. Gore, Introduction to space-time wireless communications, Cambridge University Press 2003.
[7] J.-S. Jiang and M.A. Ingram, "Spherical-wave model for short-range MIMO," IEEE Trans. Commun., vol.53, no.9, pp.1534–1541, Sept. 2005.
[8] L. Liu, W. Hong, H. Wang, G. Yang, N. Zhang, H. Zhao, J. Chang, C. Yu, X. Yu, H. Tang, H. Zhu, and L. Tian, "Characterization of line-of-sight MIMO channel for fixed wireless communications," Antennas Wirel. Propag. Lett., vol.6, no.11, pp.36–39, March 2007.
[9] F. Bøhagen, P. Orten, and G.E. Øien, "Design of optimal high-rank line-of-sight MIMO channels," IEEE Trans. Wireless Commun., vol.6, no.4, pp.1420–1425, April 2007.
[10] I. Sarris and A.R. Nix, "Design and performance assessment of high-capacity MIMO architectures in the presence of a line-of-sight component," IEEE Trans. Veh. Technol., vol.56, no.4, pp.2194–2202, July 2007.
[11] H. Hirayama, G. Matsui, N. Kikuma, and K. Sakakibara, "Channel capacity improvement in short-range MIMO using side and back reflectors," IEICE Trans. Commun., vol.E94-B, no.5, pp.1280–1283, May 2011.
[12] D. Zhang, T. Hori, and M. Fujimoto, "Channel capacity improvement in near-field MIMO system using metal wires," IEICE Trans. Commun., vol.E96-B, no.5, pp.1141–1148, May 2013.
[13] M.R. Andrews, P.P. Mitra, and R. deCarvalho, "Tripling the capacity of wireless communications using electromagnetic polarization," Nature, vol.409, no.6818, pp.316–318, Jan. 2001.
[14] K. Hiraga, T. Seki, K. Nishimori, and K. Uehara, "Effectiveness of short-range MIMO using dual-polarized antenna," IEICE Trans. Commun., vol.E95-B, no.1, pp.87–96, Jan. 2012.
[15] K. Hiraga, K. Sakamoto, K. Nishimori, T. Seki, T. Nakagawa, and K. Uehara, "A study of short-range MIMO transmission utilizing polarization multiplexing for the simplification of decoding," IEICE Trans. Commun., vol.E97-B, no.2, pp.459–468, Feb. 2014.
[16] Y. Tak and S. Nam, "Mode-based computation method of channel characteristics for a near-field MIMO," Antennas Wirel. Propag. Lett., vol.10, pp.1170–1173, Oct. 2011.
[17] M.A. Nikravan, H.G. Schantz, A.H. Unden, and D.-H. Kwon, "Channel multiplexing technique utilizing electric and magnetic components of a radio wave," IEEE Commun. Lett., vol.18, no.2, pp.317–320, Feb. 2014.
[18] R. Kataoka, K. Nishimori, T. Hiraguri, N. Honma, T. Seki, K. Hiraga, and H. Makino, "Analog decoding method for simplified short-range MIMO transmission," IEICE Trans. Commun., vol.E97-B, no.3, pp.620–630, March 2014.
[19] K. Sakamoto, K. Hiraga, T. Seki, T. Nakagawa, and K. Uehara, "Performance evaluation of short-range MIMO using a method for controlling phase difference between each propagation channel," IEICE Trans. Commun., vol.E96-B, no.10, pp.2513–2520, Oct. 2013.
[20] M. Arai, K. Hiraga, T. Nakagawa, T. Seki, and K. Uehara, "Theoretical and experimental analysis of spatial division using antenna directivities in short-range MIMO transmission," Electron. Lett., vol.50, no.2, pp.65–67, Jan. 2014.
[21] K. Hiraga, T. Nakagawa, M. Arai, K. Sakamoto, T. Seki, K. Uehara, and H. Toshinaga, "Study on MIMO transmission using orthogonal directivities obtained from higher order microstrip antenna modes," Electron. Lett., vol.50, no.7, pp.562–564, April 2014.
[22] K. Murata, N. Honma, K. Nishimori, and H. Morishita, "Analog eigenmode transmission for short-range MIMO," IEEE Trans. Veh. Technol., 2015 (in press).
[23] K. Murata, N. Honma, K. Nishimori, and H. Morishita, "Bidirectional matching technique for Tx and Rx ports in short-range MIMO," Asia-Pacific Microwave Conference (APMC 2014), pp.498–500, Nov. 2014.
[24] K. Murata, H. Morishita, N. Honma, K. Nishimori, and D.M. Klymyshyn, "Analog-digital hybrid eigenmode transmission for massive short-range MIMO," 2014 IEEE International Workshop on Electromagnetics (iWEM), pp.223–224, 2014.
[25] K. Murata, N. Honma, K. Nishimori, and H. Morishita, "Analog eigenmode transmission for 2×2 short-range MIMO," 2014 IEEE Antennas and Propagation Society International Symposium (APSURSI), pp.476–477, 2014.
[26] K. Murata, N. Honma, M. Tsunezawa, K. Nishimori, and H. Morishita, "Experimental evaluation of analog eigenmode transmission for short-range MIMO: Array parameter independency and wideband characteristics," IEICE Communications Express, vol.4, no.6, pp.198–204, April 2015.
[27] D.M. Pozar, Microwave Engineering, 4th ed., Wiley, New York, 2012.
[28] G.R. Simpson, "A generalized n-port cascade connection," MTT-S International Microwave Symposium Digest, pp.507–509, 1981.
[29] E. Hammerstad and Ø. Jensen, "Accurate models for microstrip computer-aided design," MTT-S International Microwave Symposium Digest, pp.407–409, 1980.
[30] J.C. Coetzee and Y. Yu, "Port decoupling for small arrays by means of an eigenmode feed network," IEEE Trans. Antennas Propag., vol.56, no.6, pp.1587–1593, June 2008.
[31] J.H. Kim and W.S. Park, "A Hadamard matrix feed network for a dual-beam forming array antenna," IEEE Trans. Antennas Propag., vol.57, no.1, pp.283–286, Jan. 2009.
[32] D.M. Klymyshyn, M. Börner, D.T. Haluzan, E.G. Santosa, M.

Schaffer, S. Achenbach, and J. Mohr, "Vertical high-Q RF-MEMS devices for reactive lumped-element circuits," IEEE Trans. Microw. Theory Techn., vol.58, no.11, pp.2976–2986, Nov. 2010.

[33] M. Vargas and R. Pallàs-Areny, "Thermal noise in a finite bandwidth," IEEE Instrum. Meas. Mag., vol.4, no.4, pp.23–25, Dec. 2001.

[34] Mentor Graphics. The IE3D^{TM} electromagnetic design. [Online]. http://www.mentor.com/electromagnetic-simulation/

[35] K. Hiraga, T. Seki, K. Nishimori, K. Nishikawa, I. Toyoda, and K. Uehara, "Analyses of antenna displacement in short-range MIMO transmission over millimeter-wave," IEICE Trans. Commun., vol.E94-B, no.10, pp.2891–2895, Oct. 2011.

Appendix:

In this appendix, the causes of the capacity deterioration by AE-SDM compared to DE-SDM are discussed. The possible main causes are considered as the following two factors; 1) receiving power decrease by insertion loss of CCCs and 2) interference increase due to the impurity of the channel orthogonality. In the following consideration, experimental and simulation results when d is 1.0 λ are used for the evaluation of each characteristic.

A.1 Receiving Power Decrease by Insertion Loss of CCCs

For the purpose of evaluating the performance deterioration caused by the insertion loss of CCCs, transmission characteristics when Tx and Rx CCCs directly connected were measured as shown in Fig. A· 1. In the result, it is found that the average transmission power is −0.77 dB per each stream, that should be ideally 0 dB. This deterioration is attributed to copper and reflection losses of Tx and Rx CCCs and cables used for connecting CCCs. Thus, characteristics when assuming that insertion loss can be compensated are evaluated in following parts, and the channel matrix when insertion loss of CCCs is compensated, $\boldsymbol{S}_{\mathrm{chl,\,comp}}$, is expressed as

$$\boldsymbol{S}_{\mathrm{chl,\,comp}} = \frac{\boldsymbol{S}_{\mathrm{chl,\,meas}}}{\sqrt{\left\|\boldsymbol{S}_{\mathrm{chl,\,thr}}\right\|_F^2 / N_{\mathrm{Tx}}}} \qquad (\mathrm{A}\cdot 1)$$

where $\boldsymbol{S}_{\mathrm{chl,\,meas}}$ is a experimentally-measured channel matrix when CCCs are connected to Tx and Rx sides and $\left\|\boldsymbol{S}_{\mathrm{chl,\,thr}}\right\|_F$ is the Frobenius norm of a transmission matrix measured when Tx and Rx CCCs are directly connected.

Figure A· 2 shows the norm of the channel matrix, or transmission power. In the figure, open and filled markers represent without CCCs and with CCCs, respectively. And stars represent characteristics of the compensated channel matrix. From the figure, although the norm characteristic is deteriorated when CCCs are connected, the transmission power with CCCs is raised to the same level as that without CCCs by compensating for the insertion loss. Figure A· 3 shows channel capacity characteristics, and it is confirmed that channel capacity is also improved by compensating for the insertion loss. However, unlike the norm characteristics shown in Fig. A· 2, even though the insertion loss is compensated, capacity characteristics with compensation does not match those without CCCs and are still slightly lower.

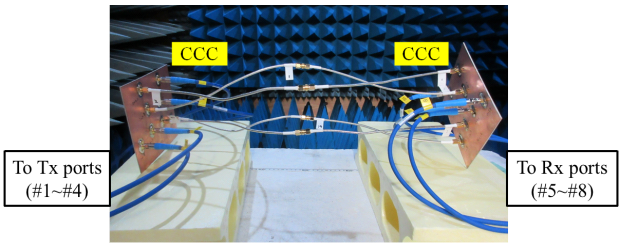

Fig. A· 1 Measurement of through characteristics of Tx-Rx CCCs.

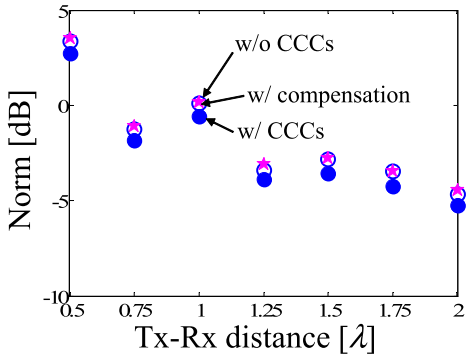

Fig. A· 2 Norm characteristics with insertion loss compensation.

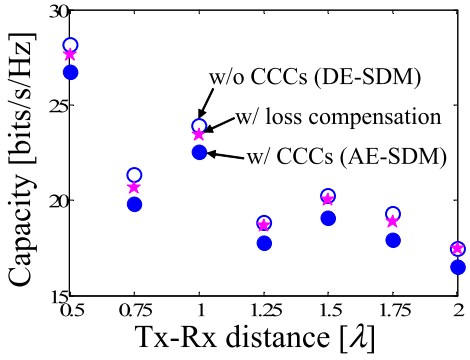

Fig. A· 3 Capacity characteristics with insertion loss compensation.

A.2 Impurity of Channel Orthogonality

Next, capacity degradation caused by impurity of channel orthogonality is considered. As mentioned in 2, if ideal CCCs are connected to a perfectly plane-symmetrically configured MIMO system, interference channels from non-corresponding Tx ports to a certain Rx port theoretically become zero. However, because of manufacturing error of CCCs and MSA arrays and array displacement, it is practically difficult to perfectly realize the regular symmetrical channel matrix expressed as (2). Thus, these factors deteriorate purity of channel orthogonality resulting in an increase of interference power. According to the Table 1, the prototype of CCCs were manufactured with high dimensional accuracy, therefore, it is regarded that impurity of channel orthogonality is mainly due to the influences of the Tx and

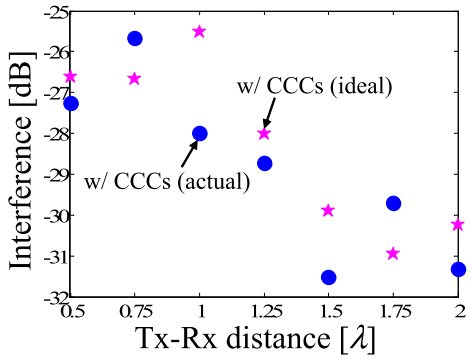

Fig. A· 4 Interference characteristics with ideal CCCs.

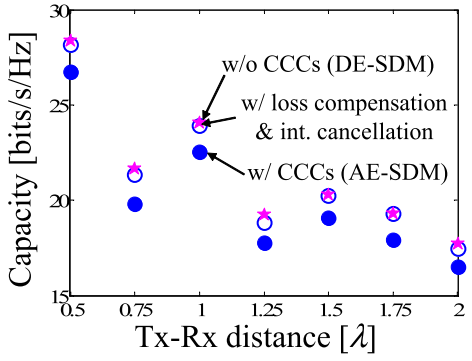

Fig. A· 5 Capacity characteristics with insertion loss compensation and ideal interference cancellation.

Rx MSA arrays configuration such as fabrication and displacement errors.

First, interference power characteristics are evaluated in case that ideal CCCs are connected to the SR-MIMO system by post-processing. If the SR-MIMO system including Tx and Rx arrays is perfectly configured plane-symmetrically, ideal CCCs enable complete interference suppression. The analysis result is shown in Fig. A· 4, and stars represent characteristics when ideal CCCs applied to a measured channel matrix without CCCs. Also, interference characteristics calculated from the measured channel matrix with actual CCCs are shown with filled circles for comparison. From the result, it is confirmed, even though ideal CCCs are used, interferences still remain at the same level as that with the actual CCCs. This indicates that channel orthogonality is spoiled by not so much manufacturing error of CCCs but the asymmetry of SR-MIMO array configuration.

Then, it is assumed that it is possible to cancel the remaining interference completely which cannot be suppressed by manufactured CCCs. In analysis, the interference is canceled by applying DE-SDM by post-processing to a measured channel matrix with CCCs. In Fig. A· 5, capacities with both loss compensation and interference cancellation are plotted with stars and almost agree with that of ideal DE-SDM plotted with open circles as can be seen from the figure.

A.3 Some Countermeasures and Future Work

In summary, if 1) the CCCs are fabricated with more accuracy and less losses, and 2) the arrays are plane-symmetrically positioned more precisely, the channel capacity closer to that of ideal DE-SDM can be achieved by AE-SDM. Largely, the asymmetry of the channel matrix due to array displacement, inclination and the presence of environmental scatterers is critical for the proposed technique. In particular, an SR-MIMO at millimeter wave frequency is sensitive to such factors since, for example, several-centimeter displacement could be several wavelengths [35].

To address such factors causing the asymmetrical channel, several approaches were suggested and their robustnesses against asymmetrical channel condition were evaluated. In the technique suggested in [19], power and phase differences between channels are controlled by using sub-arrays with variable attenuators to regenerate a quasi-ideal channel condition. Reference [21] proposed a channel orthogonalization technique by using multiple MSAs operating at different higher-order modes and reported that it was robust to a certain level of fading; this technique is similar to our proposed technique in that the orthogonal directivities are employed for multiplexing [22]. In our future work, we also need to evaluate the robustness of the proposed technique and consider some countermeasures for non-ideal cases.

Kentaro Murata received the B.E. and M.E. degrees in electrical and electronics engineering from Iwate University, Morioka, Japan in 2011 and 2014, respectively. He is currently working toward the Ph.D. degree with Graduate School of Science and Engineering, National Defense Academy of Japan, Yokosuka, Japan. His current research interests include feeding methods for multiple-input-multiple-output antenna systems.

Naoki Honma received the B.E., M.E., and Ph.D. degrees in electrical engineering from Tohoku University, Sendai, Japan in 1996, 1998, and 2005, respectively. In 1998, he joined the NTT Radio Communication Systems Laboratories, Nippon Telegraph and Telephone Corporation (NTT), in Japan. He is now working for Iwate University. He received the Young Engineers Award from the IEICE of Japan in 2003, the APMC Best Paper Award in 2003, the Best Paper Award of IEICE Communication Society in 2006, and the APMC Best Paper Award in 2014, respectively. His current research interest is MIMO antennas for high-speed wireless communication systems.

Kentaro Nishimori received the B.E., M.E. and Ph.D. degrees in electrical and computer engineering form Nagoya Institute of Technology, Nagoya, Japan in 1994, 1996 and 2003, respectively. In 1996, he joined the NTT Wireless Systems Laboratories, Nippon Telegraph and Telephone Corporation (NTT), in Japan. He was senior research engineer on NTT Network Innovation Laboratories. He is now associate professor in Niigata University. He was a visiting researcher at the Center for Teleinfrastructure (CTIF), Aalborg University, Aalborg, Denmark from Feb. 2006 to Jan. 2007. He was an Associate Editor for the Transactions on Communications for the IEICE Communications Society from May 2007 to May 2010 and Assistant Secretary of Technical Committee on Antennas and Propagation of IEICE from June 2008 to May 2010. He received the Young Engineers Award from the IEICE of Japan in 2001, Young Engineer Award from IEEE AP-S Japan Chapter in 2001, Best Paper Award of Software Radio Society in 2007 and Distinguished Service Award from the IEICE Communications Society in 2005, 2008 and 2010. His main interests are spatial signal processing including MIMO systems and interference management techniques in heterogeneous networks. He is a member of IEEE and IEICE. He received IEICE Best Paper Award in 2010.

David M. Klymyshyn was born in Yorkton, Canada in 1968. He received his B.E., M.Sc., and Ph.D. degrees in Electrical Engineering from the University of Saskatchewan, Canada in 1990, 1995, and 1998, respectively. From 1990 to 1994, Dr. Klymyshyn was with SED Systems (Canada), and in 1995 was with WaveCom Electronics (now Vecima Networks-Canada), where he was involved in the design of various commercial microwave satellite and communication systems. From 1998–2013 he was a Research Scientist with Telecommunication Research Labs (Canada) where he received 7 "Professor Performance Awards" for graduate supervision in microwave/wireless research. He also has ongoing research collaboration with the Institute of Microstructure Technology, Karlsruhe Institute of Technology (KIT-Germany), where he was a Visiting Scientist in 2004 and 2008. Since 1998, he has been a Professor of Electrical and Computer Engineering at the University of Saskatchewan (UofS), teaching undergraduate and graduate microwave courses. Dr. Klymyshyn has supervised more than 50 students and researchers, and has received 11 "Merit Awards" for research and scholarly work at the UofS. He was selected as a "Rising Star" by the VP Research at UofS, and was nominated for the "Ivany Internationalization Award". In 2012, Dr. Klymyshyn was awarded a Discovery Accelerator Supplement grant from the Natural Sciences and Engineering Research Council of Canada (NSERC) to recognize "a superior research program", one "highly rated for originality and innovation". He has 4 patents and 5 pending patents in the microwave/antenna area. Dr. Klymyshyn's current research interests focus on microwave/antenna devices and circuits fabricated in thick materials. His group was first in Canada to demonstrate fabrication of high-aspect-ratio RF MEMS reactive devices and circuits, polymer-based dielectric resonator antenna structures, and artificial dielectric structures and antennas fabricated using deep X-ray lithography. He is co-Principal Investigator at Canada's deep XRL facility, SyLMAND (Synchrotron Laboratory for Micro/Nano Devices). Dr. Klymyshyn has published over 110 papers, including a *Journal of Micromechanics and Microengineering* paper in the "Year's Best Papers from 2010", and an IEEE Antennas and Propagation Magazine paper awarded the "2012 IEEE Edward E. Altshuler Year's Best Paper Award".

Hisashi Morishita received the B.S. degree in Electrical Engineering from National Defense Academy of Japan in 1980, the M.S. and Ph.D. degrees from University of Tsukuba in 1987 and 1990, respectively. From 1990 to 1992, he worked as a research and development officer at Air Research and Development Command of Japan Air Self-Defense Force (JASDF). Since 1992, he has been with National Defense Academy and is currently a Professor in the Department of Electrical and Electronic Engineering. From 1996 to 1997, he was a Visiting Researcher at the Communications Research Laboratory, McMaster University, Canada. His research is concerned with mobile communication and small antennas. He is a fellow of IEICE and a senior member of IEEE.